Reactor characterization and primary application of a state of art dual-reactor chamber in the investigation of atmospheric photochemical processes

*Hao Luo, Guiying Li, Jiangyao Chen, Yujie Wang, Taicheng An**

Guangdong Key Laboratory of Environmental Catalysis and Health Risk Control, Guangzhou Key Laboratory Environmental Catalysis and Pollution Control, School of Environmental Science and Engineering, Institute of Environmental Health and Pollution Control, Guangdong University of Technology, Guangzhou 510006, China

ARTICLE INFO

ABSTRACT

Increasing attention has been paid to the air pollution more recently. Smog chamber has been proved as a necessary and effective tool to study atmospheric processes, including photochemical smog and haze formation. A novel smog chamber was designed to study the atmospheric photochemical reaction mechanism of typical volatile organic compounds (VOCs) as well as the aging of aerosols. The smog chamber system includes an enclosure equipped with black lights as the light source, two parallel reactors (2 m^3 of each) with separate control of light source and temperature, with a series of coupled instruments for online monitoring of gas phase and particle phase reactants and products. Chamber characterization, including air source stability, effective light intensity, temperature stability, as well as gas phase and particle phase wall losses, were carried out before further research. The results showed that our smog chamber systems developed by other domestic and international groups. It was also observed that the wall loss of aromatic VOCs varied with different functional groups as well as the isomerism. The results of preliminary simulation experiment from styrene-NO$_x$ demonstrated that the chamber can be well utilized to simulate gas-particle conversion progresses in the atmosphere.

© 2020 The Research Center for Eco-Environmental Sciences, Chinese Academy of Sciences. Published by Elsevier B.V.

Introduction

In recent years, the increasingly prominent problems of the air pollution attract more and more public attention during the fast economic development. In the atmosphere, the degradation of volatile organic compounds (VOCs) may lead to ozone (O$_3$) and secondary organic aerosol (SOA) formations through the photochemical processes, which may further result in some pollution problems (Deng et al., 2019; Han et al., 2019; Wu et al., 2017). In general, pollution profiles can be investigated through traditional field observation and the Master Chemical Mechanism, MCMv3.2 model (http://mcm.leeds.ac.uk/MCM) (Saunders et al., 2003). This model was frequently applied to simulate the photochemical process of pollutants in the air. However, the obtained results are varied among the different research groups, since, in traditional field observation, the environmental conditions such as emissions, meteorology, mixing effects, are uncontrollable factors (Cocker III et al., 2001; Hamilton et al., 2011; Hildebrandt et al., 2009; Hynes et al., 2005; Jang and Kamens, 2001; Li et al., 2018;

Martín-Reviejo and Wirtz, 2005; Wang et al., 2011; White et al., 2014). Comparatively, the smog chambers can overcome the above-mentioned problem effectively to be used for conducting and assessing the atmospheric oxidation mechanisms of typical atmospheric pollutants and the formation of secondary pollutants (Akimoto et al., 1979; Carter et al., 1982; Jeffries et al., n.d.; Jeffries et al., 1985), due to the independently controlled variables in chamber system. In general, the size of the designed smog chamber varies from dozens of liters to dozens of cubic meters with single or dual-reactors for different purpose (Cocker III et al., 2001; Luo et al., 2019; Wang et al., 2016). Nevertheless, the dual-reactor chamber is recognized as an advanced type of smog chamber because it is independent of initial experimental conditions to simulate diverse atmospheric processes at the same time. For example, the oxidation mechanisms of aromatic precursors could be affected with the addition of methyl group in monocyclic aromatic hydrocarbon (Li et al., 2016). Cater et al. built a dual-reactor smog chamber at University of California, Riverside (UCR) and compared their dual-reactor chamber for mechanism evaluation under low NO_x concentration with the predictions of the SAPRC-99 chemical mechanism (Carter et al., 2005). Lee et al. also constructed a dual-reactor smog chamber at the Korea Institute of Science and Technology (KIST) to investigate the correlation between light intensity and O_3 formation during photochemical reactions of urban air in Seoul and proposed the correlation can be used to predict the daytime O_3 concentration (Lee et al., 2010). A single-reactor may restrict the application of the chambers. For instance, the experiments in single-reactor chamber would be unrepeatable if use the outdoor air as background gas for the changes over time. Meanwhile, a dual-reactor chamber can also be used to compare the experiments with only one key different parameter. Compared with the single-reactor smog chambers, dual-reactor chamber has proven to be more repeatable and practicable to simulate diverse atmospheric processes at the same time.

The smog chamber application researches were also carried out in domestic (Luo et al., 2019; Wang et al., 2015; Wang et al., 2014; Wang et al., 2016; Wu et al., 2007; Xu et al., 2006) and international groups (Carter et al., 2005; Lee et al., 2010) in recent decades. A 350 L fluorinated ethylene propylene (FEP) chamber was constructed (Xu et al., 2006) and much bigger chamber was used to investigate the O_3 and SOA formation (Jia and Xu, 2013, 2017; Jia et al., 2012; Wang et al., 2016). However, small volume (<1 m^3) smog chamber is more flexible to operate, but its wall losses may be relatively larger. Wu et al. studied SOA formation in a 2 m^3 FEP smog chamber in the Tsinghua University (TSC) and further evaluated the reproducibility of their chamber with others by comparing the SOA yield from toluene/NO_x photolysis (Wu et al., 2007). A few cubic meters of smog chamber is now widely accepted as an effective way to simulate atmospheric chemical reactions. In addition, a much bigger chamber (30 m^3) was also constructed at Guangzhou Institute of Geochemistry, Chinese Academy Sciences (GIG-CAS), with good reproducibility of α-pinene ozonolysis (Wang et al., 2014). The condition in larger volume is closer to the real atmosphere, but it also has the disadvantage of making the experiment take longer. Recently, a dual-reactor chamber at Institute of Chemistry, Chinese Academy of Sciences (ICCAS) was also built and characterized, considering the light source and wall loss (Wang et al.,

2015). However, the dual-reactor chamber facilities in China are still limited, although dual-reactor chamber is one of the ideal tools to efficiently compare the runs of experiments with single variable key parameter.

In this study, a new indoor dual-reactor smog chamber was built at the Guangdong University of Technology, China, and this dual-reactor chamber (GDUT-DRC) was designed to aim to investigate the gas-phase oxidation mechanism as well as secondary particle formation and aerosol aging. The facility, the instruments and the characterization are described first, and a series of characterization was conducted for new chamber, including temperature stability, irradiation light stability, and the wall loss of gas species as well as particles. Furthermore, the primary application experiments were also carried out to study the typical VOCs to particle conversion during the photooxidation of styrene in the presence of NO_x.

1.   Experiments and methods

1.1.   Facility and instruments

The GDUT-DRC facility illustrated in Fig. 1 is housed in a 10 m × 8 m × 3.5 m laboratory at the fifth floor. The facility consists of three major functional components: the reaction chamber, the pre-processing system, and the detection system. The reaction chamber involves an enclosure, two pillow shaped reactors, the light source system, and the control cabinet. The pre-processing system consists of air purification and injection systems. The detection system includes instruments to detect both gas phase and particle phase reactants and products.

1.1.1.   Enclosure
The dimension of the enclosure is 6 m × 2.5 m × 2.8 m. The inner enclosure walls are covered with reflective thin aluminum alloy sheets to obtain a maximum and uniform light intensity. High efficiency ionizing blower (varied from 0 to a maximum of 2000 r/min) can eliminate static of the dual-reactors and mix the air inside the reactors evenly. Two air conditioners in the laboratory keep uniform temperature needed in the reactors. There are regular cooling holes at the top of the enclosure. Two temperature probes are installed at the top of the enclosure. After turning on the lights and the ionizing blower, the temperature reaches a stable state, and does not change with the distance from the light. In this study, all experiments were carried out at a preset temperature of 301.15 ± 1.0 K.

1.1.2.   Dual Teflon reactor
Referring to the materials used to make smog chamber in previous studies (Carter et al., 2005; Cocker III et al., 2001; Wang et al., 2015; Wang et al., 2014), FEP was selected as the materials for GDUT-DRC reactors, pipelines and connection parts, so as to minimize the wall loss of typical VOCs and avoid releasing needless VOCs. The GDUT-DRC has two 2 m^3 pillow shaped reactors (2.5 m × 2.0 m) hanging separately on a movable aluminum alloy frame (2.0 m × 1.5 m × 2.5 m). The dual-reactors are made of 4 mil FEP Teflon film (FEP 100, DuPont, USA), which is chemically inert, optical transmissive and flexible enough to keep it under atmospheric pressure inside the reactor during inflating and pumping. Three Teflon ports of 6 mm in diameter are stretched to the middle of each reactor. The left
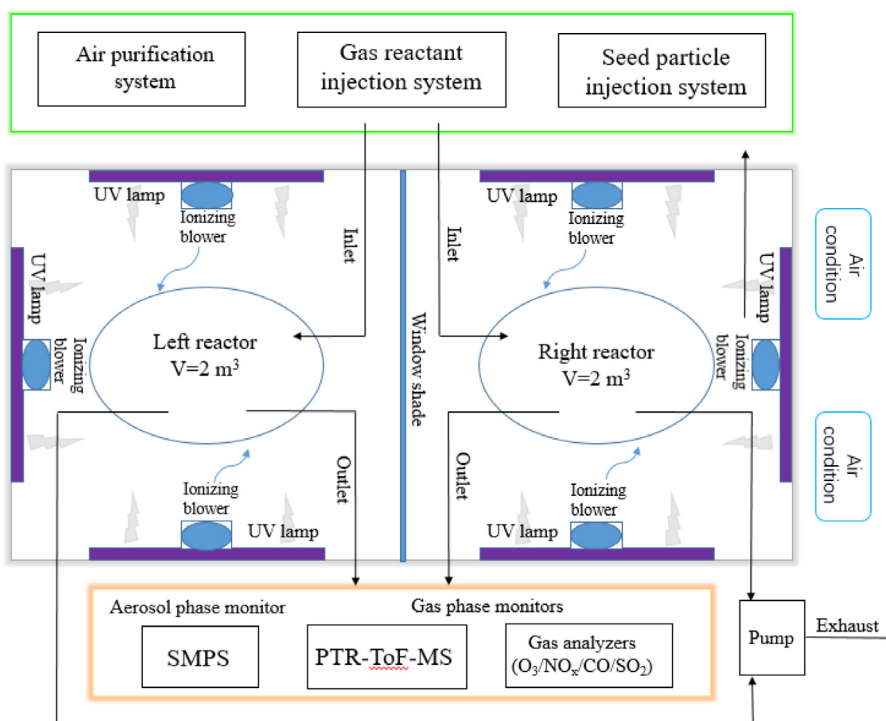
Fig. 1 – Schematic diagram of the GDUT-DRC system.

port is used for injection of purified air and seed aerosols. The middle port is used for sampling gas species. The right port is used for sampling particles and exhaust air. The reactors are cleaned between the two sample injections by brushing with flowing purified compressed air continuously under UV light irradiation for 12 hr. After purification, no remaining gas (hydrocarbons, NO, NO_2, O_3) or particles could be detected by our instruments in the reactors.

1.1.3. Light source

Generally, the UV lamps are used in chamber experiments for the high cost-effectiveness (Carter et al., 2005; Cocker III et al., 2001; Luo et al., 2019; Wang et al., 2016; Wu et al., 2007). Similar to the classical smog chambers (Jia and Xu, 2018; Luo et al., 2019; Zhang et al., 2019), GDUT-DRC are equipped with a total of 120 narrow-band black lamps (40W, F40BL, GE, USA) with a center wavelength of 365 nm. Total of 60 black lamps are evenly arranged in three banks as the light source in each reactor. The 60 black lamps in each reactor are divided into 6 independently controlled groups so that the light intensity can be conducted at different levels. A window shade mounted between the dual-reactors to cut off the UV light. The light spectra of UV lamps in the GDUT-DRC were measured using an irradiation spectrometer (Jaz spectral sensing suite, Ocean Optics Inc., USA). The light intensity in the smog chamber could also be represented by the NO_2 photolysis rate (Cocker III et al., 2001), due to the photolysis of NO_2 under the sunlight irradiation is the chain-initiating reaction for the formation of photochemical smog. NO_2 is injected into a clean reactor and then irradiated with UV light irradiation after standing for an hour to diffuse the NO_2 uniformly. According to a previous work, NO and O_3 could be produced during the NO_2 photolysis (Harvey et al., 2012). Therefore, the concentrations of NO, NO_2 and O_3 were measured immediately and continuously during

photolysis using NO_x analyzer (Model 42i, Thermo Scientific, USA) and O_3 analyzer (Model 49i, Thermo Scientific, USA). The photolysis rate, J_{NO2} (min^{-1}), of NO_2 is estimated by a steady-state actinometry according as following Eq. (1) (Harvey et al., 2012):

$$J_{NO2} = k_{NO+O3}[O_3][NO]/[NO_2] \tag{1}$$

where $[O_3]$, $[NO]$, and $[NO_2]$ are their corresponding concentrations (ppb) and k_{NO+O3} represents the rate constant (cm^3/molecule/min) of NO and O_3 reaction (Atkinson et al., 2004; Cocker III et al., 2001).

1.1.4. Air purification system and injection system

Zero air generated by Model 111 and Model 1150 (Thermo Scientific, USA, relative humidity (RH) ≤5%) which are supplied as the matrix gas and carrier gas, respectively. The purified dry air has a maximum flow rate of 50 L/min, with no detectable particles, < 0.5 ppb non-methane hydrocarbon (NMHC), and < 1 ppb NO_x, O_3 and carbonyl compounds. The RH of pure air is approximately 5%. To obtain a specific higher RH, the purified dry air is bubbling passed through a bottle with ultrapure water (18.2 MΩ cm) before introducing into the reactor, which can be varied RH from 5% to 90%. In this paper, all experiments were carried out at the RH lower than 10%.

The gas reactants (NO_x, SO_2, CO, HCs) are injected into the reactor using airtight syringes (Shanghai Anting, China) through a T-junction connected to a FEP line and spread with the flow of purified dry air. For the introduction of liquid reactants, known volumes of the reactants were injected by microliter syringes (Shanghai Anting, China) and introduced into the chamber with an injection port similar to that of used in gas reactants. O_3 is produced by combining Model 146i with Model 111 and Model 1150 (Thermo Scientific, USA). Aerosol seed particles are generated by a constant output atomizer

(Model 3076, TSI Inc., USA), and then passed through a diffusion dryer filled with allochroic silica gels and an aerosol neutralizer (Model 3082, TSI Inc., USA) before introducing into the reactors.

1.1.5. Detection system

The gas-phase and particle-phase monitors are listed and briefly described in Table S1. The concentrations of O_3, SO_2 and CO are monitored in real time using O_3 analyzer (Model 49i, Thermo Scientific, USA), SO_2 analyzer (Model 43i, Thermo Scientific, USA) and CO analyzer (Model 48i, Thermo Scientific, USA), respectively. The mixing ratio of NO_x (NO, NO_2, NO_x) is measured using a NO_x analyzer (Model 42i, Thermo Scientific, USA). All these instruments are calibrated weekly using a Thermo Scientific Model 146i multi-gas calibrator.

The concentrations of VOCs were monitored through proton transfer reaction time-of-flying mass spectrometry (PTR-ToF-MS, Ionicon Analytik, Austria). PTR-ToF-MS allows for real-time detection and quantification with high sensitivity, high time resolution (at the level of millisecond) and limits of detection down to parts-per-trillion (pptv). Some trace concentrations of inorganic gas (NH_3) and several kinds of VOCs (certain alkanes, alkene, aromatics, aldehydes, ketones, alcohols, and carboxylic acids) were detected with different primary ions (H_3O^+, O_2^+, and NO^+). Part of gas-phase intermediates can also be measured using PTR-ToF-MS.

Submicron number size distributions of formed aerosols are determined using a scanning mobility particle sizer (SMPS) equipped with an electrostatic classifier (EC, Model 3082, TSI Inc., USA), a long differential mobility analyzer (DMA, Model 3081, TSI Inc., USA) or an alternative short DMA (Model 3085, TSI Inc., USA) and a condensation particle counter (CPC, Model 3776, TSI Inc., USA). Flow rates of sheath and aerosol flow setting value are 3.0 and 0.3 L/min, respectively, allowing for a size distribution scan ranging from 13.8 to 723.4 nm within 180 s.

1.2. Wall loss

In a finite volume reactor, the particle wall loss are inevitable and cannot be neglected, since there is particle deposition onto the wall of the reactor influenced by diffusion and the charged wall (Wang et al., 2014). The particle phase wall loss can be described by a first-order kinetics as follows as Eq. (2) (Bowman et al., 1997; Cocker III et al., 2001):

$$\frac{dN(Dp, t)}{dt} = -KN(Dp)N(Dp, t) \tag{2}$$

where Dp is the diameter of the particle (nm), $N(Dp, t)$ is the particle number concentration (number/cm³), and $KN(Dp)$ is the particle number loss coefficient (min⁻¹) (Bowman et al., 1997; Cocker III et al., 2001). The $KN(Dp)$ values are obtained on the basis of the particle number concentration versus time data for each experiment.

Usually, ammonium sulfate seed particles have been used widely as reference aerosols for evaluating the particle phase wall losses (Keywood et al., 2004; Wang et al., 2015; Wang et al., 2014). Therefore, ammonium sulfate was also used as reference aerosols in our study. Approximately 0.5 mol/L ammo-

nium sulfate solution was atomized by a constant output atomizer (Model 3076, TSI Inc., USA) and injected into the reactors at a flow rate of 0.5 L/min for 10 min.

1.3. SOA formation yield

The yield of SOA is calculated by the formula as follows (Odum et al., 1996):

$$\gamma_{(SOA)} = \triangle_{(particle\ mass\ concentration)} / \triangle_{(styrene)} \tag{4}$$

where, $\gamma_{(SOA)}$ is the yield of SOA; $\triangle_{(particle\ mass\ concentration)}$ means the corrected mass concentration of particles after peak O_3 time ($\mu g/m^3$); $\triangle_{(styrene)}$ represents the reacted amount of styrene after peak O_3 time ($\mu g/m^3$).

Previously, Odum et al. found that the two product semi-empirical method could fit the yield data well under appropriate values for α_1, $K_{om,1}$, α_2, $K_{om,2}$ (Odum et al., 1996). In this model, two products represent a class of low vapor pressure compounds and a class of the higher ones, respectively. The $\gamma_{(SOA)}$ data are analyzed using the method outlined by (Odum et al., 1996). Concisely, the SOA yield is defined as the ratio of aerosol generated to hydrocarbon reacted:

$$\gamma_{(SOA)} = \Sigma_i \gamma_{i(SOA)} = M_0 \Sigma_i (\alpha_i K_{om,i} / (1 + K_{om,i} M_0)) \tag{5}$$

where, $\gamma_{(SOA)}$ is the yield of SOA, M_0 is the total mass concentration of organic material ($\mu g/m^3$), α_i and $K_{om,i}$ are the mass-based stoichiometric coefficient and the partitioning coefficient of species i.

2. Results and discussions

2.1. Characterization of the smog chamber

In order to obtain the fundamental parameters, such as temperature stability, irradiation light stability, and the wall loss of gas species and particles, the characterization of the GDUT-DRC was performed firstly.

2.1.1. Temperature stability

Fig. 2 shows the evolutions of the temperatures measured in the two reactors under the UV light irradiation (light spectrum: range from 335 to 415 nm and the same peak intensity at 367 nm; light intensity: left: 0.163 min⁻¹, right: 0.168 min⁻¹). The ideal preset temperature is 301.15 K under UV lamp irradiation. Before the light irradiation, the temperatures were recorded as 295.55 and 295.35 K in the left and right reactors, respectively. Once the UV lights were on, the temperatures increased sharply up to 300.15 K within initial 50 min, and then rose slowly to the preset temperature (301.15 K) as the irradiation time increasing from 50 to 120 min. After initial swift increasing, the measured temperatures of the left and right reactors tended to reach steady state at 301.15 ± 0.2 and 301.25 ± 0.3 K within approximately 90 min and thereafter, indicating that the chamber can maintain the preset temperature stably. In conclusion, it indicated that the temperature in our chamber can be preset steadily to perform the subsequent experiments effectively.
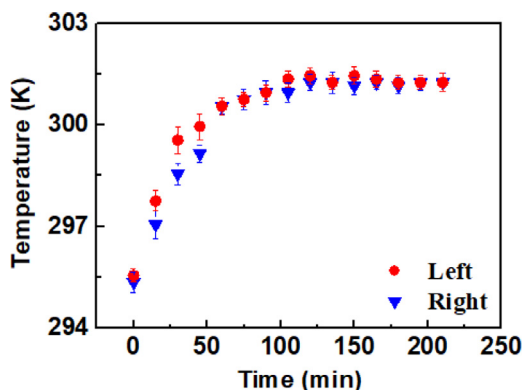
Fig. 2 – Evolutions of temperature in the two reactors of GDUT-DRC under the UV light irradiation (light spectrum: range from 335 to 415 nm and the peak intensity at 367 nm; light intensity: left: 0.163 min⁻¹; right: 0.168 min⁻¹). The setting temperature is 28.0°C.

Fig. 4 – Comparison of the rate constant of particle wall loss in the GDUT-DRC and other chambers (ICCAS-DRC (Wang et al., 2015) and GIG-CAS chamber (Wang et al., 2014)).
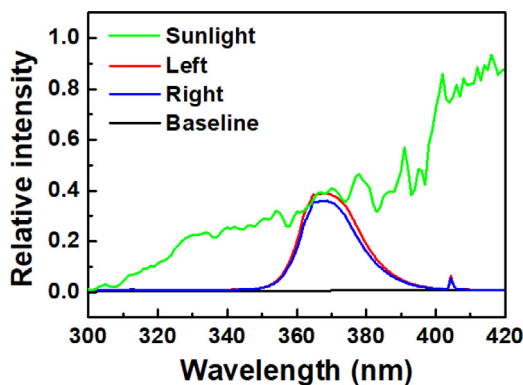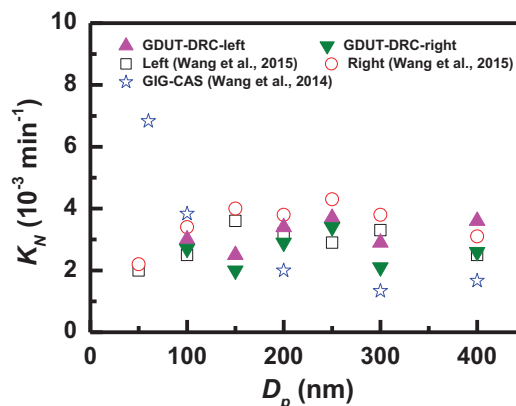

Fig. 3 – Measured spectrum of sunlight and black lamps in two reactors of GDUT-DRC system.

2.1.2.   Light spectrum and intensity stability

As shown in Fig. 3, the light spectrum of UV lights and sunlight at GDUT (113°24′18.31″N, 23°2′34.41″E) at afternoon of August 5, 2017 were measured. The baseline indicated that there is no light source in the dual-reactors when the UV-lights were turned off. In contrast, when the UV-lights were turned on, the dual-reactors have the similar irradiation range from 335 to 415 nm with the peak intensity at 367 nm. After a wavelength of over 400 nm, only a few negligible peaks were observed. It is noticed that the spectrum of UV light is similar to the sunlight in the range of 360-380 nm. As shown in Fig. S1, the initial NO_2 concentration in both left and right reactors is set as 150 ppb. After turning on the UV lamps, with a sharp decrease of the NO_2 concentration, the concentrations of NO and O_3 concurrently increased sharply within the first 5 min and then reached equilibrium. Meanwhile, similar results were observed in the parallel experiments, indicating that the light source in GDUT-DRC is stable enough for performing the follow-up photooxidation experiments. As demonstrated in Fig. S2, the photolysis rates of NO_2 in the right reactor are all slightly higher than that in the left reactor. After correction for the dark NO and O_3 reaction in the sampling tube, the average J_{NO2} values of GDUT-DRC are obtained to be 0.161 min⁻¹ for the left reactor and 0.169 min⁻¹ for the right reactor, respec-

tively. Therefore, in general, the light source intensity of the two reactors in GDUT-DRC is very close, which can effectively realize the control variables in parallel experiments. Comparatively, the photolysis rates of NO_2 in other chamber were also shown as follows: left: 0.153 min⁻¹; right: 0.139 min⁻¹ (Wang et al., 2015). Thus, we can observe that our GDUT-DRC system has a more stable light source. In conclusion, the light source conditions in the left and right reactors of GDUT-DRC are very similar and stable, which can be applied in subsequent experiments.

2.1.3.   Wall loss of gas phase compounds and particle

The wall loss in chamber is one of the key issues in experimental characterization, which has an impact on gas-phase reactivity and secondary organic aerosol formation (Hu et al., 2014; Wang et al., 2015; Wang et al., 2014). Therefore, the wall loss of the gaseous compounds (NO_2, NO, O_3) in the GDUT-DRC were also evaluated by monitoring the concentration attenuation of these compounds under dark condition. The average wall loss rate constants of NO_2, NO, O_3 in GDUT-DRC and other chambers are all listed and compared in Table 1. In our GDUT-DRC system, the wall loss rate constants of NO_2, NO, O_3 are as follows: left: 0.5×10^{-4} min⁻¹, 0.3×10^{-4} min⁻¹, 3.3×10^{-4} min⁻¹; right: 0.3×10^{-4} min⁻¹, 0.3×10^{-4} min⁻¹, 2.7×10^{-4} min⁻¹. Obviously, the wall loss rate constants of the dual-reactors in our chamber are very close and are all of the same order of magnitudes as other smog chambers (Bloss et al., 2005; Grosjean, 1985; Metzger et al., 2008; Wang et al., 2015; Wang et al., 2014; Wu et al., 2007). Thus, it indicating that the wall loss rate constants of the dual-reactors in our chamber are reliable and within acceptable range, and can be used to correct measured concentrations in the subsequent experiments. As shown in Fig. 4, the wall loss rate constants of 100-400 nm particle were also determined to be in the range of 2.1×10^{-3} - 3.7×10^{-3} min⁻¹, while the total number loss rate constant was obtained as 2.4×10^{-3} min⁻¹ for the right reactor, and 2.9×10^{-3} min⁻¹ for the left reactor, respectively. These results are also close to the previous studies (McMurry and Grosjean, 1985; Wang et al., 2015; Wang et al., 2014), which indicating that the particle phase wall loss in our chamber system is also within the acceptable range. Therefore, in conclusion, the wall losses of both gas and particle in

Table 1 – Comparison of wall loss rate constants of gas species in GDUT-DRC with other chambers.

Species	Wall loss rate(10^{-4} min^{-1})				GIG-CAS[b]	TSC[c]	ERT[d]	PSI[e]	EUPHORE[f]
	GDUT-DRC		ICCAS-DRC[a]						
	Left	Right	Left	Right					
O_3	3.3	2.7	3.1	2.5	1.31	6.10	0.5-3.0	2.40	1.8
NO	0.3	0.3	3.1	3.0	1.41	0.38	0.0-5.4	NA[g]	NA
NO_2	0.5	0.3	4.5	3.8	1.39	0.42	0.0-2.0	0.13-2.52	NA
VOC	0.24	0.19	0.31	0.3	ND[h]	0.07	NA	NA	NA

[a] (Wang et al., 2015); [b] (Wang et al., 2014); [c] (Wu et al., 2007); [d] (Grosjean, 1985); [e] (Metzger et al., 2008); [f] (Bloss et al., 2005); [g] NA = not applicable; ND[h] = not detetable
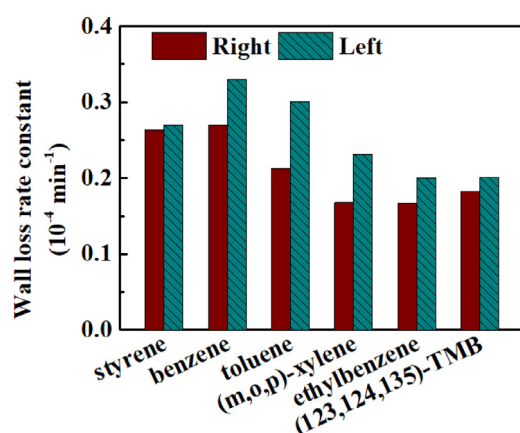
Fig. 5 – Contrast of the wall loss rate constant of different aromatic VOCs with different groups in the GDUT-DRC. Xylene: (m, o, p)-Xylene; TMB: (123, 124, 135)-trimethylbenzene.

our chamber are in the reasonable range, and it is credible to study photochemical gas-particle transformation.

2.1.4.   Wall loss of VOCs

The wall loss of VOCs is also an important factor in the characterization of smog chamber. In this study, a series of aromatic VOCs were employed as references for the investigation of VOCs wall loss. The wall loss rate constants of aromatic VOCs in GDUT-DRC are conducted and illustrated in Fig. S3, which ranged from 0.18×10^{-4} to 0.34×10^{-4} min^{-1} in the left reactor and from 0.16×10^{-4} to 0.26×10^{-4} min^{-1} in the right reactor, respectively. Compared with the wall loss of NO_2 and O_3, there is a similar characteristic that the wall loss of the left reactor is a little higher than that of the right reactor. This demonstrates that the wall losses of left and right reactors are close. However, the wall losses of isomers in the measured aromatic VOCs varied in values. For example, the order of the wall losses of trimethylbenzene (TMB) is as follows: 124-TMB > 123-TMB > 135-TMB; the order of wall loss of xylene: m-xylene > o-xylene > p-xylene. As shown in Fig. 5, the wall losses varied in aromatic VOCs with different groups. The order of wall loss of aromatics VOCs with different groups is shown as follows: benzene (styrene) > toluene > xylene > ethylbenzene > trimethylbenzene. This phenomenon indicated that

the wall loss rate of aromatic VOCs may be related to the substituent group on the benzene ring. So far, we have found no other studies to report the same results. As shown in Table 1, the average VOCs wall losses were obtained as 0.24×10^{-4} and 0.19×10^{-4} min^{-1} in the left and right reactor respectively. In the previous studies of smog chambers, due to the different selected species or measurement methods, the wall losses of measured VOCs varied greatly (Grosjean, 1985; Wang et al., 2015; Wang et al., 2014; Wu et al., 2007). When propylene is used commonly as the representative VOC species for wall loss measurement, the rate constant is basically one order of magnitude smaller than that of conventional gas species (NO_2, NO, and O_3) (Wang et al., 2015). However, the VOCs wall losses in our GDUT-DRC system are slightly lower than that of the other smog chamber, demonstrating that the VOC wall loss in our chamber is reliable. In conclusion, the wall loss rate constants of aromatic VOCs in GDUT-DRC are within acceptable range and can be used to balance VOC concentrations in the subsequent experiments.

2.2.   Primary application in photooxidation of styrene-NO_x under different VOC/NO_x

The photooxidation experiments of styrene-NO_x were preliminarily carried out to simulate the gas-particle conversion processes in this GDUT-DRC system without aerosol seed, and the initial condition is shown in Table 2. After 12 hr cleaning with UV-light, 2 m^3 reactor was filled with zero air (RH < 10%), then NO_2 and styrene were successively introduced with zero air flow into the reactor. The VOC/NO_x ratio was adjusted, and a series of photooxidation experiments of styrene-NO_x were carried out. As the reaction progressed, the concentrations of NO_2 decreased rapidly in the first 30 min and then began to decline slowly. In contrast, the concentrations of O_3 and NO rose and then gradually stabilized at the same time scale. These indicate that NO_x (NO_2 and NO) and O_3 can reach an equilibrium state within 30 min during the photooxidation of styrene-NO_x (The initial conditions were demonstrated as follows: left reactor: styrene: 562 ppb; NO: 5.3 ppb; NO_2: 155.2 ppb; right reactor: styrene: 534 ppb; NO: 5.7 ppb; NO_2: 158.7 ppb). As shown in Fig. 6, obviously, the experiment results in both reactors are in good agreements with the model values of Master Chemical Mechanism, MCMv3.2 model, via website: http://mcm.leeds.ac.uk/MCM. This proves that our GDUT-DRC system can effectively simulate VOC photochemical experi-

Table 2 – Experimental conditions of styrene-NO$_x$ photooxidation.

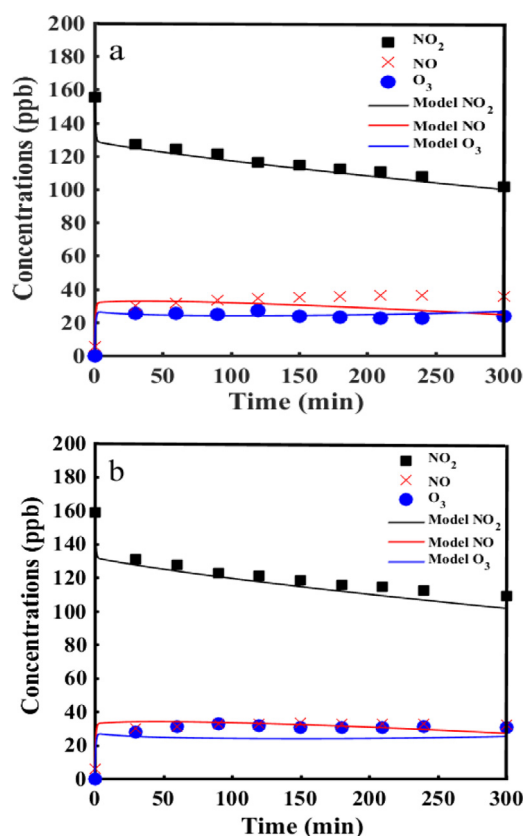| Styrene (ppb)	NO$_x$ (ppb)	VOC/NO$_x$	△SOA (μg/m^3)	Yeild	T (K)
221	156.6	1.41	1.27	0.004884	303.15
410	165.9	2.47	1.33	0.003167	304.15
562	160.0	3.51	5.91	0.008166	303.65
629	170.7	3.68	5.69	0.010969	303.15
750	163.1	4.60	3.66	0.008479	304.15
866	163.0	5.31	4.42	0.016497	303.15
955	165.7	5.76	8.57	0.026602	303.15
948	167.7	5.65	10.43	0.023503	303.15
1020	164.9	6.19	13.48	0.042943	304.15
1040	169.0	6.15	26.94	0.049895	303.65

Fig. 6 – Comparison of O$_3$ and NO$_x$ from the photooxidation of styrene-NO$_x$ between the MCM model and our observed results (Initial condition: (a) left reactor: styrene: 562 ppb; NO: 5.3 ppb; NO$_2$: 155.2 ppb; (b) right reactor: styrene: 534 ppb; NO: 5.7 ppb; NO$_2$: 158.7 ppb)

Fig. 7 – Secondary organic aerosol (SOA) yields for styrene-NO$_x$ experiments and comparison with previous studies (Ma et al., 2018; Na et al., 2006).

ments. However, there are some minor deviations in these two reactors, which the deviations of left reactor are relatively smaller. The little deviations of NO, NO$_2$ and O$_3$ may attribute to the measurement uncertainties between these two reactors. In conclusion, GDUT-DRC can be used to accurately simulate VOCs photooxidation experiment.

In the photooxidation of styrene-NO$_x$, the SOA yield varies from 0.5% to 5.0%. This demonstrates that the gas-particle transformation in the photochemical reaction of styrene can be successfully simulated in our GDUT-DRC system. The comparison of SOA yields for styrene-NO$_x$ photo-oxidation experiments of this work compared with other previous stud-
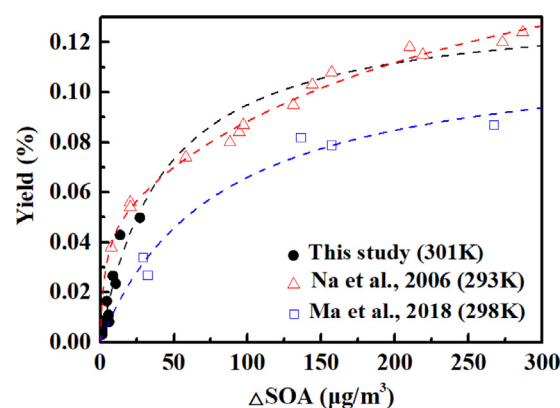
ies (Ma et al., 2018; Na et al., 2006) is all illustrated in Fig. 7. The optimal parameters in the present study are α_1=0.12794, $K_{om,1}$=0.02357, α_2=0.00743, $K_{om,2}$=0.02354, respectively. The yield curve fits well with our experiment data at temperature of 301 K, which is also comparable with the yield data at temperature of 293 K (Na et al., 2006), but higher than the yield at temperature of 298 K (Ma et al., 2018). However, this is most probably because our assumed aerosol density of 1.4 g/cm^3 is slightly higher than the previous studies when calculating aerosol mass concentrations (Ma et al., 2018; Na et al., 2006). In conclusion, the agreement between our SOA yield data and many previous studies demonstrated that the chamber system fabricated in the present study is able to accurately simulate secondary organic aerosol formation.

3.   Conclusions

A new dual-reactor chamber facility was designed and built to study atmospheric VOCs photooxidation progresses in this study. Effective on-line monitoring technology of gas phase and particle phase has been equipped in our GDUT-DRC system. A series of initial characterization experiments have been carried out to demonstrate that the wall losses of gas phase and particle phase in our GDUT-DRC system are small, which show good agreement with other's early reported chambers. The results of the preliminary experiments of VOCs photooxidation as well as SOA formation illustrate that GDUT-DRC is able to be used for simulating gas-particle partitioning pro-

cesses. Furthermore, the experimental and simulation results show good reproducibility and demonstrate its ability to provide valuable data for the study of gas-particle conversion processes.

Declaration of Competing Interest

None.

Acknowledgement

Appendix A Supplementary data

Supplementary material associated with this article can bey found, in the online version, at doi:10.1016/j.jes.2020.05.021.

REFERENCES

Akimoto, H., Hoshino, M., Inoue, G., Sakamaki, F., Washida, N., Okuda, M., 1979. Design and characterization of the evacuable and bakable photochemical smog chamber. Environ. Sci. Technol. 13, 471–475.

Atkinson, R., Baulch, D.L., Cox, R.A., Crowley, J.N., Hampson, R.F., Hynes, R.G., et al., 2004. Evaluated kinetic and photochemical data for atmospheric chemistry: volume I - gas phase reactions of Ox, HOx, NOx and SOxspecies. Atmos. Chem. Phys. 4 (6), 1461–1738.

Bloss, C., Wagner, V., Jenkin, M.E., Volkamer, R., Bloss, W.J., Lee, J.D., et al., 2005. Development of a detailed chemical mechanism (MCMv3.1) for the atmospheric oxidation of aromatic hydrocarbons. Atmos. Chem. Phys. 5, 641–664.

Bowman, F.M., Seinfeld, J.H., Pandis, S.N., 1997. Mathematical modelling for gas-particle partitioning of secondary organic aerosols. Atmos. Environ. 31, 3921–3931.

Carter, W.P.L., Atkinson, R., Winer, A.M., Pitts Jr, J.N., 1982. Experimental investigation of chamber-dependent radical sources. Int. J. Chem. Kinet. 14, 1071–1103.

Carter, W.P.L., Cocker III, D.R., Fitz, Malkina, I.L., Bumiller, K., Sauer, C.G., et al., 2005. A new environmental chamber for evaluation of gas-phase chemical mechanisms and secondary aerosol formation. Atmos. Environ. 39 (40), 7768–7788.

Cocker III 3rd, D.R., Flagan, R.C., Seinfeld, J.H., 2001. State-of-the-art chamber facility for studying atmospheric aerosol chemistry. Environ. Sci. Technol. 35 (12), 2594–2601.

Deng, Y., Li, J., Li, Y., Wu, R., Xie, S., 2019. Characteristics of volatile organic compounds, NO$_2$, and effects on ozone formation at a site with high ozone level in Chengdu. J. Environ. Sci. 75, 334–345.

Grosjean, D., 1985. Wall loss of gaseous pollutants in outdoor Teflon chambers. Environ. Sci. Technol. 19 (11), 1059–1065.

Hamilton, J.F., Rami Alfarra, M., Wyche, K.P., Ward, M.W., Lewis, A.C., McFiggans, G.B., et al., 2011. Investigating the use of secondary organic aerosol as seed particles in simulation chamber experiments. Atmos. Chem. Phys. 11 (12), 5917–5929.

Han, C., Liu, R., Luo, H., Li, G., Ma, S., Chen, J., An, T., 2019. Pollution profiles of volatile organic compounds from different urban functional areas in Guangzhou China based on GC/MS and PTR-TOF-MS: atmospheric environmental implications. Atmos. Environ. 214, 116843.

Harvey, R.B., Stedman, D.H., Chameides, W., 2012. Determination of the absolute rate of solar photolysis of NO$_2$. J. Air Pollut. Control Assoc. 27 (7), 663–666.

Hildebrandt, L., Donahue, N.M., Pandis, S.N., 2009. High formation of secondary organic aerosol from the photo-oxidation of toluene. Atmos. Chem. Phys. 9 (9), 2973–2986.

Hu, C.J., Cheng, Y., Pan, G., Gai, Y.B., Gu, X.J., Zhao, W.X., et al., 2014. A smog chamber facility for qualitative and quantitative study on atmospheric chemistry and secondary organic aerosol. Chin. J. Chem. Phys. 27 (6), 631–639.

Hynes, R., Angove, D., Saunders, S., Haverd, V., Azzi, M., 2005. Evaluation of two MCM v3.1 alkene mechanisms using indoor environmental chamber data. Atmos. Environ. 39 (38), 7251–7262.

Jang, M., Kamens, R.M., 2001. Characterization of secondary aerosol from the photooxidation of toluene in the presence of NOx and 1-propene. Environ. Sci. Technol. 35, 3626–3639.

Jeffries, H.E., Kamens, R.M., Sexton, K.G., Gerhardt, A.A., 1982. Outdoor smog chamber experiments to test photochemical models.

Jeffries, H.E., Sexton, K.G., Kamens, R.M., Holleman, M.S., 1985. Outdoor smog chamber experiments to test photochemical models: phase II. Final Rep..

Jia, L., Xu, Y., 2013. Effects of relative humidity on ozone and secondary organic aerosol formation from the photooxidation of benzene and ethylbenzene. Aerosol Sci. Technol. 48 (1), 1–12.

Jia, L., Xu, Y., 2017. Different roles of water in secondary organic aerosol formation from toluene and isoprene. Atmos. Chem. Phys. Discuss. 1–43.

Jia, L., Xu, Y., 2018. Different roles of water in secondary organic aerosol formation from toluene and isoprene. Atmos. Chem. Phys. 18 (11), 8137–8154.

Jia, L., Xu, Y., Shi, Y., 2012. Investigation of the ozone formation potential for ethanol using a smog chamber. Chin. Sci. Bull. 57 (34), 4472–4481.

Keywood, M.D., Varutbangkul, V., Bahreini, R., Flagan, R.C., Seinfeld, J.H., 2004. Secondary organic aerosol formation from the ozonolysis of cycloalkenes and related compounds. Environ. Sci. Technol. 38, 4157–4164.

Lee, S.B., Bae, G.N., Lee, Y.M., Moon, K.C., Choi, M., 2010. Correlation between light intensity and ozone formation for photochemical smog in urban air of Seoul. Aerosol Air Qual. Res. 10 (6), 540–549.

Li, K., Chen, L., White, S.J., Yu, H., Wu, X., Gao, X., et al., 2018. Smog chamber study of the role of NH$_3$ in new particle formation from photo-oxidation of aromatic hydrocarbons. Sci. Total Environ. 619–620, 927–937.

Li, L., Tang, P., Nakao, S., Chen, C.L., Cocker III, D.R., 2016. Role of methyl group number on SOA formation from monocyclic aromatic hydrocarbons photooxidation under low-NOx conditions. Atmos. Chem. Phys. 16 (4), 2255–2272.

Luo, H., Jia, L., Wan, Q., An, T., Wang, Y., 2019. Role of liquid water in the formation of O3 and SOA particles from 1,2,3-trimethylbenzene. Atmos. Environ. 217, 116955.

Ma, Q., Yu, H., Yang, C.Q., Lin, X.X., Gai, Y.B., Zhang, W.J., 2018. Influence of 2-butanol on secondary organic aerosol formation from ozonolysis of styrene: Experimental and model studies. Acta Sci. Circum. 38, 3888–3893.

Martín-Reviejo, M., Wirtz, K., 2005. Is benzene a precursor for secondary organic aerosol. Environ. Sci. Technol. 39, 1045–1054.

McMurry, P.H., Grosjean, D., 1985. Gas and aerosol wall losses in Teflon film smog chambers. Environ. Sci. Technol. 19 (12), 1176–1182.

Metzger, A., Dommen, J., Gaeggeler, K., Duplissy, J., Prevot, A.S.H., Kleffmann, J., et al., 2008. Evaluation of 1,3,5 trimethylbenzene degradation in the detailed tropospheric chemistry mechanism, MCMv3.1, using environmental chamber data. Atmos. Chem. Phys. 8 (21), 6453–6468.

Na, K., Song, C., Cocker III, D.R., 2006. Formation of secondary organic aerosol from the reaction of styrene with ozone in the presence and absence of ammonia and water. Atmos. Environ. 40 (10), 1889–1900.

Odum, J.R., Hoffmann, T., Bowman, F., Collins, D., C, F.R., Seinfeld, J.H., 1996. Gas/particle partitioning and secondary organic aerosol yields. Environ. Sci. Technol. 30, 2580–2585.

Saunders, S.M., Jenkin, M.E., Derwent, R.G., Pilling, M.J., 2003. Protocol for the development of the master chemical mechanism, MCM v3 (Part A): tropospheric degradation of non-aromatic volatile organic compounds. Atmos. Chem. Phys. 3, 161–180.

Wang, J., Doussin, J.F., Perrier, S., Perraudin, E., Katrib, Y., Pangui, E., et al., 2011. Design of a new multi-phase experimental simulation chamber for atmospheric photosmog, aerosol and cloud chemistry research. Atmos. Meas. Tech. 4 (11), 2465–2494.

Wang, W.G., Li, K., Zhou, L., Ge, M.F., Hou, S.Q., Tong, S.R., et al., 2015. Evaluation and application of dual-reactor chamber for studying. Acta Phys. Chim. Sin. 31 (7), 1251–1259.

Wang, X., Liu, T., Bernard, F., Ding, X., Wen, S., Zhang, Y., et al., 2014. Design and characterization of a smog chamber for studying gas-phase chemical mechanisms and aerosol formation. Atmos. Meas. Tech. 7 (1), 301–313.

Wang, Y., Luo, H., Jia, L., Ge, S., 2016. Effect of particle water on ozone and secondary organic aerosol formation from benzene-NO2-NaCl irradiations. Atmos. Environ. 140, 386–394.

White, S.J., Jamie, I.M., Angove, D.E., 2014. Chemical characterisation of semi-volatile and aerosol compounds from the photooxidation of toluene and NOx. Atmos. Environ. 83, 237–244.

Wu, S., Lü, Z., Hao, J., Zhao, Z., Li, J., Takekawa, H., et al., 2007. Construction and characterization of an atmospheric simulation smog chamber. Adv. Atmos. Sci. 24 (2), 250–258.

Wu, W., Zhao, B., Wang, S., Hao, J., 2017. Ozone and secondary organic aerosol formation potential from anthropogenic volatile organic compounds emissions in China. J. Environ. Sci. 53, 224–237.

Xu, Y., Jia, L., Ge, M., Du, L., Wang, G., Wang, D., 2006. A kinetic study of the reaction of ozone with ethylene in a smog chamber under atmospheric conditions. Chin. Sci. Bull. 51 (23), 2839–2843.

Zhang, Q., Xu, Y., Jia, L., 2019. Secondary organic aerosol formation from OH-initiated oxidation of m-xylene: effects of relative humidity on yield and chemical composition. Atmos. Chem. Phys. Discuss. 1–22.